

In-medium ω mass from the $\gamma + Nb \rightarrow \pi^0\gamma + X$ reaction

M. Nanova¹, V. Metag¹, G. Anton², J.C.S. Bacelar³, O. Bartholomy⁴, D. Bayadilov^{4,5}, Y.A. Beloglazov⁵, R. Bogendörfer², R. Castelijns³, V. Crede^{4,a}, H. Dutz⁶, A. Ehmans⁴, D. Elsner⁶, K. Essig⁴, R. Ewald⁶, I. Fabry⁴, M. Fuchs⁴, Ch. Funke⁴, R. Gothe^{6,b}, R. Gregor¹, A.B. Gridnev⁵, E. Gutz⁴, S. Höffgen⁴, P. Hoffmeister⁴, I. Horn⁴, J. Hösler², I. Jaegle⁷, J. Junkersfeld⁴, H. Kalinowsky⁴, Frank Klein⁶, Friedrich Klein⁶, E. Klempt⁴, M. Konrad⁶, B. Kopf^{8,9}, M. Kotulla¹, B. Krusche⁷, J. Langheinrich^{6,9}, H. Löhner³, I.V. Lopatin⁵, J. Lotz⁴, S. Lugert¹, D. Menze⁶, T. Mertens⁷, J.G. Messchendorp³, C. Morales⁶, R. Novotny¹, M. Ostrick^{6,c}, L.M. Pant^{1,d}, H. van Pee⁴, M. Pfeiffer¹, A. Roy^{1,e}, A. Radkov⁵, S. Schadmand^{1,f}, Ch. Schmidt⁴, H. Schmieden⁶, B. Schoch⁶, S. Shende^{3,i}, G. Suft², A. Süle⁶, V. V. Sumachev⁵, T. Szczepanek⁴, U. Thoma⁴, D. Trnka¹, R. Varma^{1,g}, D. Walther⁴, Ch. Weinheimer^{4,h}, Ch. Wendel⁴

(The CBELSA/TAPS Collaboration)

¹*II. Physikalisches Institut, Universität Gießen, Germany*

²*Physikalisches Institut, Universität Erlangen, Germany*

³*Kernfysisch Versneller Instituut Groningen, The Netherlands*

⁴*Helmholtz-Institut für Strahlen- u. Kernphysik Universität Bonn, Germany*

⁵*Petersburg Nuclear Physics Institute Gatchina, Russia*

⁶*Physikalisches Institut, Universität Bonn, Germany*

⁷*Physikalisches Institut, Universität Basel, Switzerland*

⁸*Institut für Kern- und Teilchenphysik TU Dresden, Germany*

⁹*Physikalisches Institut, Universität Bochum, Germany*

^a*Current address: Florida State University Tallahassee, FL, USA*

^b*Current address: University of South Carolina Columbia, SC, USA*

^c*Current address: Physikalisches Institut Universität Mainz, Germany*

^d*Current address: Nuclear Physics Division BARC, Mumbai, India*

^e*Current address: IIT Indore, Indore, India*

^f*Current address: Forschungszentrum Jülich, Germany*

^g*Current address: Department of Physics I.I.T. Powai, Mumbai, India*

^h*Present address: Universität Münster, Germany*

ⁱ*Current address: Department of Physics,*

Univ. of Pune, Pune, India

(Dated: November 8, 2018)

Data on the photoproduction of ω mesons on nuclei have been re-analyzed in a search for in-medium modifications. The data were taken with the Crystal Barrel(CB)/TAPS detector system at the ELSA accelerator facility in Bonn. First results from the analysis of the data set were published by D. Trnka et al. in Phys. Rev. Lett 94 (2005) 192303 [1], claiming a lowering of the ω mass in the nuclear medium by 14% at normal nuclear matter density. The extracted ω line shape was found to be sensitive to the background subtraction. For this reason a re-analysis of the same data set has been initiated and a new method has been developed to reduce the background and to determine the shape and absolute magnitude of the background directly from the data. Details of the re-analysis and of the background determination are described. The ω signal on the Nb target, extracted in the re-analysis, does not show a deviation from the corresponding line shape on a LH_2 target, measured as reference. The earlier claim of an in-medium mass shift is thus not confirmed. The sensitivity of the ω line shape to different in-medium modification scenarios is discussed.

PACS numbers: 14.40.Be, 21.65.-f, 25.20.-x

I. INTRODUCTION

Quantum Chromodynamics (QCD) has been remarkably successful in describing strong interactions at high energies ($\gg 10$ GeV) and short distances ($\leq 10^{-2}$ fm) where quarks and gluons are the relevant degrees of freedom. At these scales the strong coupling is so small ($\alpha_s \approx 0.1$) that perturbative treatments provide a first order description of the phenomena [2–4]. Applying QCD at lower energies is a major challenge. In the GeV energy range the coupling strength among quarks

and gluons becomes very large and hadrons - composite objects made of quarks and gluons - emerge as the relevant degrees of freedom. A rigorous way to solve QCD in this energy regime is lattice QCD. With the advent of high speed supercomputers remarkable progress has been achieved in lattice QCD simulations with dynamical u , d , and s quarks. Dürr et al [5] have recently succeeded in reproducing masses of mesons and baryons within 3% of the experimental values.

While the properties of free hadrons are in most cases experimentally known with reasonable accuracy a pos-

sible modification of these properties in a strongly interacting medium is a much debated issue. In fact, in-medium changes of hadron properties have been identified as one of the key problems in understanding the non-perturbative sector of QCD. Fundamental symmetries in QCD provide guidance in dealing with strong interaction phenomena in the non-perturbative domain. Furthermore, QCD sum rules have been applied to connect the quark-gluon sector to hadronic descriptions. Along these lines, QCD inspired hadronic models have been developed to calculate the in-medium self-energies of hadrons and their spectral functions. Mass shifts and/or in-medium broadening as well as more complex structures in the spectral function due to the coupling of vector mesons to nucleon resonances have been predicted. A recent overview is given in [6]. These studies have motivated widespread experimental attempts to confirm or refute these theoretical predictions.

Heavy-ion collisions and reactions with photons and protons have been used to extract experimental information on in-medium properties of hadrons. The experiments have focused on the light vector mesons ρ , ω and ϕ since their decay lengths are comparable to nuclear dimensions after being produced in some nuclear reaction. To ensure a reasonable decay probability in the strongly interacting medium cuts on the recoil momentum are, however, required for the longer lived ω and ϕ mesons.

A full consensus has not yet been reached among the different experiments. A detailed account of the current status of the field is given in comprehensive reviews [7, 8]. An in-medium broadening of the vector mesons is reported by almost all experiments and the majority of experiments does not find evidence for a mass shift. Apart from [1] only one other experiment at KEK [9] reports a drop of the ρ and ω mass by 9 % at normal nuclear matter density. Studying ω meson production in ultra-relativistic heavy-ion collisions, the NA60 collaboration observes a suppression of the meson yield for ω momenta below 1 GeV/c which is even more pronounced for more central collisions [10]. This is interpreted as evidence for in-medium modifications of slow ω mesons but it cannot be concluded whether this is due to a mass shift, a broadening, or both.

It should be noted that a search for mass shifts has turned out to be much more complicated than initially thought for those cases where a strong broadening of the meson is observed as for the ω [11] and ϕ meson [12]. In the $\omega \rightarrow \pi^0\gamma$ decay mode the increase in the total width of ω drastically lowers the branching ratio for in-medium decays into this channel and thereby reduces the sensitivity of the observed ω signal to in-medium modifications.

In this paper data on the photoproduction of ω mesons on Nb and LH_2 are re-analyzed which were taken with the CB/TAPS detector system at the ELSA accelerator facility in Bonn. First results from an analysis of these data were published by D. Trnka et al. [1], claiming a mass shift of the ω meson by -14% at normal nuclear matter density. This information was extracted from a compar-

ison of the ω signals on Nb and LH_2 , reconstructed in the $\pi^0\gamma$ channel. As pointed out in the literature [13] the deduced line shapes are very sensitive to the background subtraction. While in the initial work the background was determined by fitting the $\pi^0\gamma$ invariant mass spectrum a much more refined background determination is used in the current analysis. The paper gives a full account of the experiment and details of the analysis steps.

II. EXPERIMENTAL SETUP

A. CB/TAPS detector system at ELSA

Data on LH_2 , C , and Nb have been taken with the detector system Crystal Barrel (CB) [14] and TAPS [15, 16] at the electron stretcher facility ELSA [17, 18]. The detector setup is shown schematically in Fig. 1 left. Electrons extracted from ELSA with energy E_0 hit a primary radiation target, a thin copper or diamond crystal, and produce bremsstrahlung [19]. The energy of the bremsstrahlung photons is determined eventwise from the deflection of the scattered electrons in a magnetic field. The detector system in the focal plane of the magnet consists of 480 scintillating fibers and 14 partly overlapping scintillator bars. From the energy of the scattered electron E_e^- the energy of the photon impinging on the nuclear target is given by $E_\gamma = E_0 - E_e^-$. Photons were tagged in the energy range from 0.5 GeV up to 2.6 GeV for an incoming electron energy of 2.8 GeV. The total tagged photon intensity was about $10^7 s^{-1}$ in this energy range. The energy resolution varied between 2 MeV for the high photon energies and 25 MeV for the low photon energies, respectively. The part of the beam that did not produce any bremsstrahlung photons was deflected by the magnet as well. Since these electrons retained their full energy the curvature of their track is smaller and they passed over the tagger into a beam dump.

The Crystal Barrel (CB) detector, a photon calorimeter consisting of 1290 CsI(Tl) crystals (≈ 16 radiation lengths), covered the complete azimuthal angle and the polar angle from 30° to 168° . The LH_2 , C and Nb targets (30 mm in diameter, 53 mm, 20 mm and 1 mm thick, respectively) were mounted in the center of the CB, surrounded by a scintillating fibre-detector to register charged particles [20]. The CB was combined with a forward detector - the TAPS calorimeter - consisting of 528 hexagonal BaF₂ crystals ($\approx 12 X_0$), covering polar angles between 5° and 30° and the complete azimuthal angle. In front of each BaF₂ module a 5 mm thick plastic scintillator was mounted for the identification of charged particles. The combined CB/TAPS detector covered 99% of the full 4π solid angle. The high granularity of this system makes it very well suited for the detection of multi-photon final states.

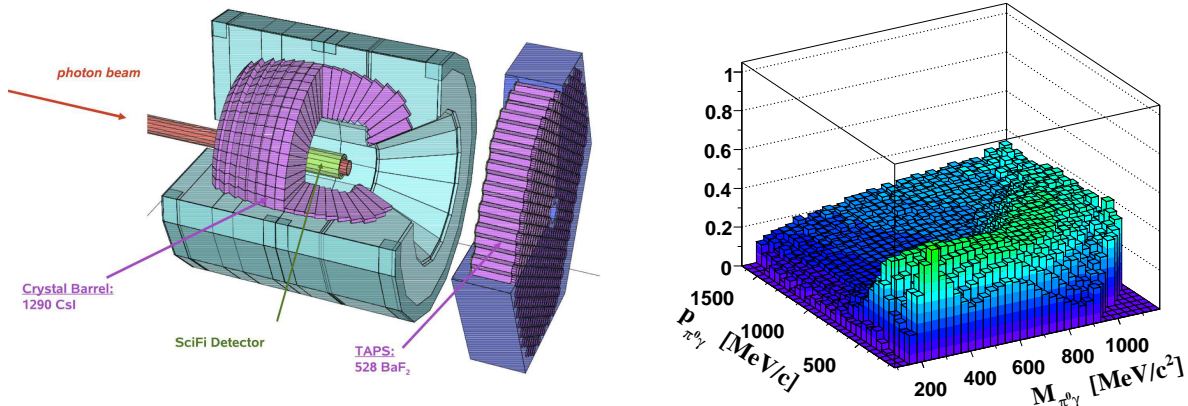


FIG. 1. (Color online) Left: Sketch of the CB/TAPS setup. The tagged photons impinge on the nuclear target in the center of the Crystal Barrel detector. The TAPS detector at a distance of 1.18 m from the target serves as a forward wall of the Crystal Barrel. The combined detector system provides photon detection capability over almost the full solid angle. Charged particles leaving the target are identified in the inner scintillating-fiber detector and in the plastic scintillators in front of each BaF₂ crystal in TAPS. Right: Detector acceptance for the $p\pi^0\gamma$ final state as a function of the invariant mass and momentum of the $\pi^0\gamma$ pair for incident photon energies of 900 to 2200 MeV.

B. The trigger

ω mesons produced by photons on a nuclear target were identified via their $\omega \rightarrow \pi^0\gamma \rightarrow \gamma\gamma\gamma$ decay. Events with ω candidates (3 photons in the final state) were selected with suitable trigger conditions: the first level trigger was derived from TAPS, requiring either ≥ 2 hits above a low threshold (A) or, alternatively, ≥ 1 hit above a high threshold (B). The second level trigger (C) was based on a fast cluster recognition (FACE) logic, providing the number n of clusters in the Crystal Barrel as well as their energy and angle within $\simeq 10 \mu\text{s}$. For the data on the solid target the total trigger condition required $[A \vee (B \wedge C)]$, with $n = 2$ clusters identified on the second level (C). Events with two photon candidates were taken for calibration purposes and for checking the analysis with known cross sections.

C. Detector acceptance

Although the CB/TAPS detector system covers almost the full solid angle it is nevertheless very important to study the acceptance for reconstructing the reaction of interest. Monte Carlo (MC) simulations of the reaction $\gamma A \rightarrow X p \pi^0 \gamma$ have been performed for solid targets using the GEANT3 package, assuming a phase space distribution of the final state particles and taking the Fermi motion of nucleons in the target nucleus into account. The reconstruction of simulated $\pi^0\gamma$ data is done for the same trigger conditions as in the experiment and for the incident photon energy range from 900 to 2200 MeV. The acceptance as a function of the invariant mass and the momentum of the $p\pi^0\gamma$ final state is shown in Fig. 1 right. In the ω mass range the acceptance is rather flat

as a function of momentum and amounts to $\approx 35\%$.

III. ANALYSIS

A. Calibration

Since the experiment searches for possibly small mass shifts it is absolutely mandatory to verify the linearity, accuracy and stability of the photon energy calibration. The accurately known masses of the π^0 and η meson are used as calibration fix points since the decay photons of π^0 and η mesons cover the full range in energy of the ω decay photons. The invariant masses of the mesons were calculated from the measured 4 momenta of the decay photons. To ensure the stability of the photon energy calibration the invariant mass of π^0 - and η -mesons is checked for different momentum bins. For this check a 2-dimensional plot of the $\pi^0(\eta)$ invariant mass against the momentum $|\vec{p}|_{\pi(\eta)}$ of the $\pi^0(\eta)$ is filled (Fig. 2a) and projected onto the $\pi^0(\eta)$ invariant mass axis for different slices in the momentum of the $\gamma\gamma$ pair. Changes in the π^0 and η meson invariant mass with momentum are found to be less than $\leq 1.9\%$ and 1.3% , respectively (Fig. 2b). The peak position of π^0 at 135 MeV and of η at 547 MeV is stable for different cuts on the momentum like > 500 MeV or < 500 MeV (Fig. 2c,d). In addition, it has been verified that the energy calibrations for the runs with different targets are in agreement. This is demonstrated in Fig. 3 which shows the signal line shapes for the π^0 and η meson measured via their two photon decays for the LH_2, C and Nb targets.

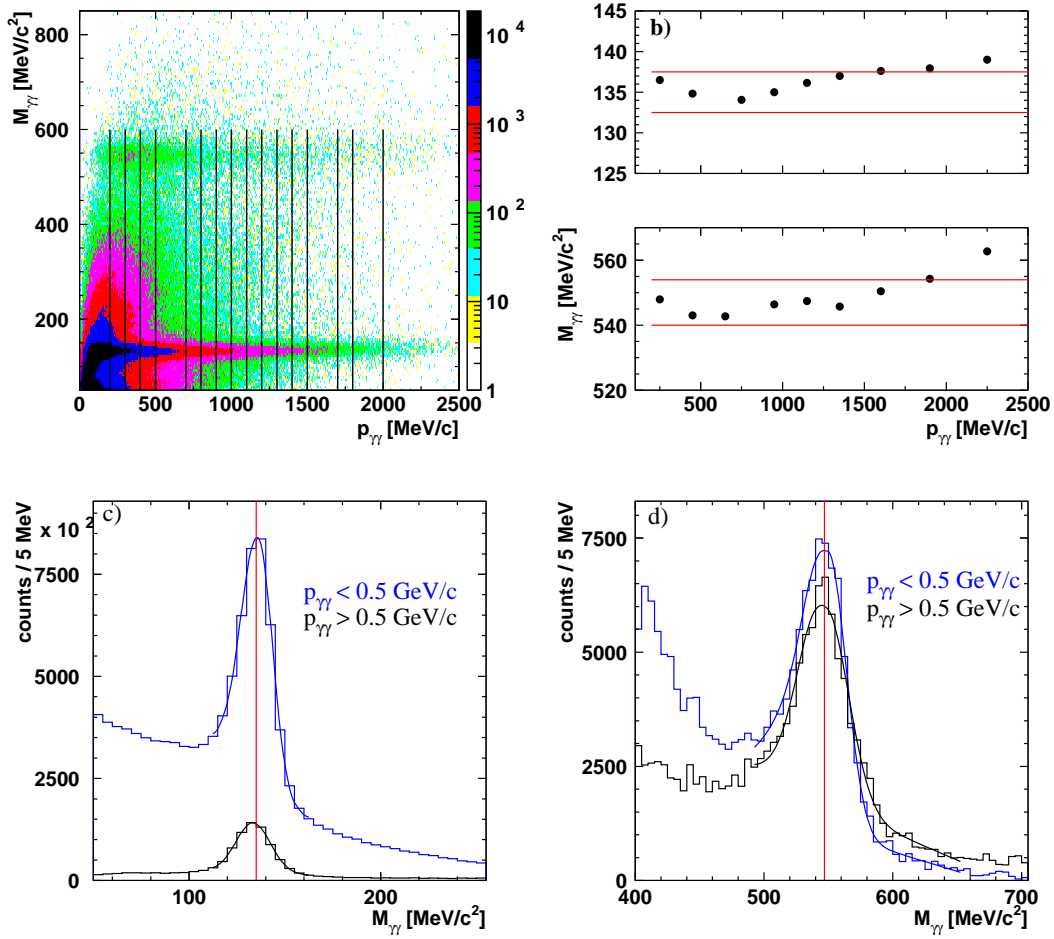


FIG. 2. (Color online) a) Invariant mass of two γ 's ($\pi^0 \rightarrow \gamma\gamma$ and $\eta \rightarrow \gamma\gamma$) as a function of the momentum of the 2γ pair for the Nb target. The vertical lines show the slices for the projections on the y-axis. b) The peak position of the π^0 and η invariant mass in 8 slices of the momentum. The horizontal lines show the tolerance of ± 2.5 MeV of the π^0 mass ($135 \text{ MeV}/c^2$) and of ± 7 MeV of the η mass ($547 \text{ MeV}/c^2$). c) The π^0 invariant mass for low and high momenta. d) The η invariant mass for low and high momenta.

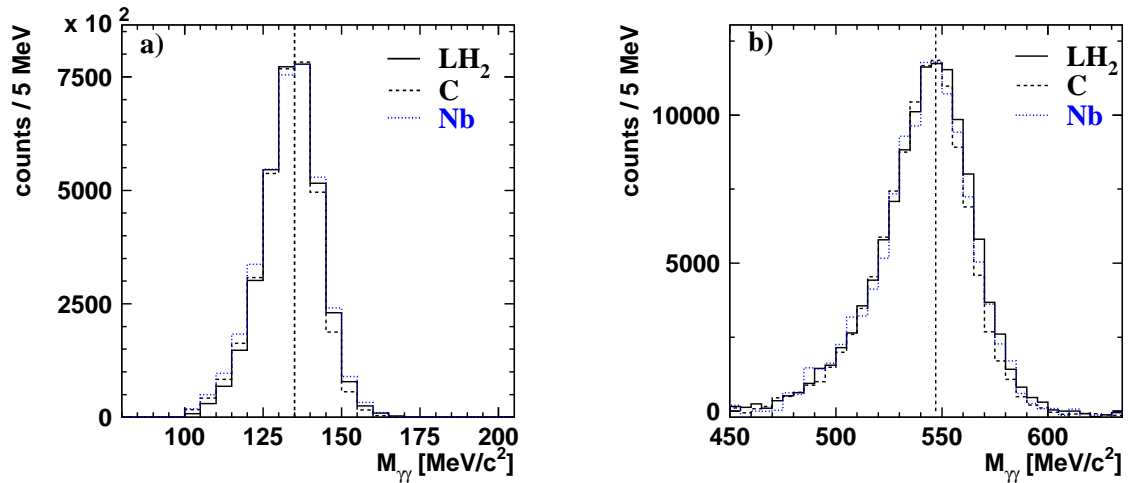


FIG. 3. (Color online) π^0 (a) and η (b) invariant mass distributions reconstructed from the $\pi^0(\eta) \rightarrow \gamma\gamma$ decay for the LH_2 , C and Nb targets after background subtraction.

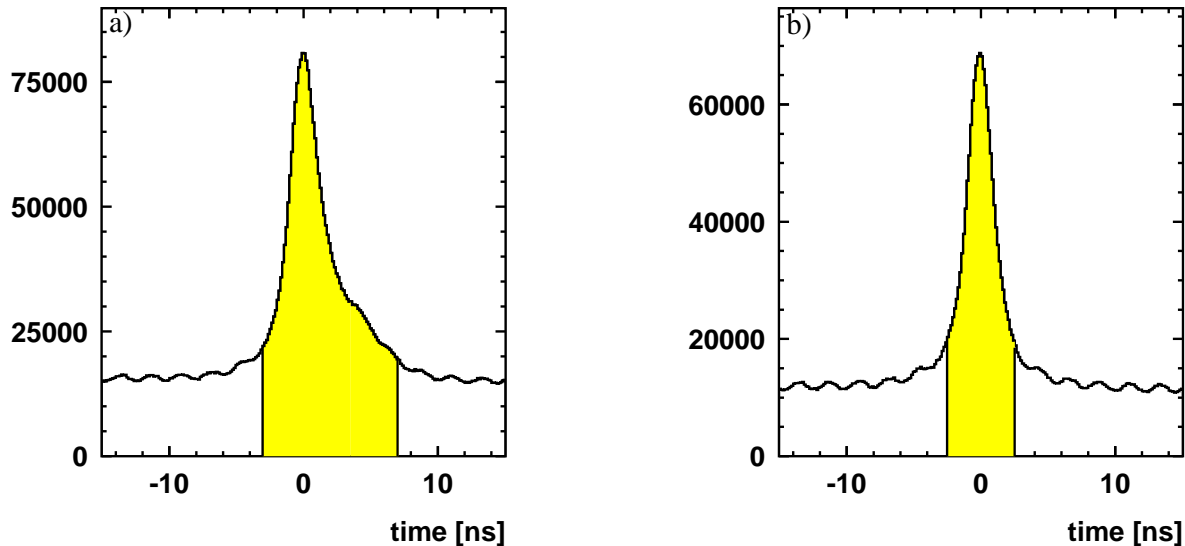


FIG. 4. (Color online) TAPS-tagger coincidence time spectra without (a) and with (b) requiring the hit in TAPS to be due to a photon (no response in plastic scintillator in front of TAPS). The shaded areas represent the applied cuts. The peaks reside on an uniformly distributed background stemming from random coincidences.

B. Event Selection

ω mesons were reconstructed in the reaction $\gamma A \rightarrow (A-1)p\omega \rightarrow (A-1)p\pi^0\gamma$ from events with 3 photons and one proton in the final state in contrast to the analysis by D. Trnka et al. [1] where the fourth particle was not further identified. In a first step only those events were selected which had 4 hits, so called PED (particle energy deposit), in the detector system. In order to reconstruct the reaction for ω photoproduction 1 charged particle was required in coincidence with 3 neutral hits (from the 4 PED data set) in the CB/TAPS detector system. The selection of the charged particles was done by using either the information from the fiber detector in the CB or the information from the plastic scintillators in front of the TAPS detector. Requesting a charged particle in addition to 3 neutral hits leads to a loss in statistics, but is essential for the background determination described in section III D.

The possible background contributions were investigated via Monte Carlo simulations. The reactions $\gamma A \rightarrow (A-1)p\pi^0\pi^0 \rightarrow (A-1)p4\gamma$ and $\gamma A \rightarrow (A-1)p\pi^0\eta \rightarrow (A-1)p4\gamma$, where one of the photons in the final state escaped detection, were found to be the dominant background sources. Furthermore the reaction $\gamma A \rightarrow (A-1)n\pi^+\pi^0$ where the neutron and the π^+ are misidentified as a photon and a proton, respectively, also contribute to the background. For the analysis which is presented here the background was reconstructed from 5 PED events with 4 neutral and 1 charged particle (see section III D).

C. Reconstruction of the ω meson

1. Incident photon energy range

The analysis was performed for incident photon energies from 900 to 2200 MeV, i.e. starting about 200 MeV below the ω production threshold off the free nucleon $E_{\gamma,thresh}^N=1109$ MeV. The threshold for ω production on nuclei is given by the threshold for coherent production

$$E_{\gamma,thresh} = m_{\omega} + \frac{m_{\omega}^2}{2m_A} \quad (1)$$

where the recoil momentum of the produced meson is taken up by the whole nucleus. For a Nb target Eq. 1 yields a coherent threshold energy of $E_{\gamma,thresh} = 786$ MeV, i.e. the threshold is even lower than 900 MeV. The choice of the incident energy interval represents a compromise between sufficiently low energies for ω production off a nuclear target and sufficient discrimination of background sources, which strongly increase with decreasing photon energies; e.g., the $2\pi^0$ channel, which is the strongest background channel, exhibits maxima in the cross section for incident photon energies near 1080 and 750 MeV.

2. Time coincidence

For reconstructing the reaction $\gamma A \rightarrow (A-1)p\omega \rightarrow (A-1)p\gamma\gamma\gamma$ a prompt coincidence between a particle in TAPS and an electron in the tagger was required to elim-

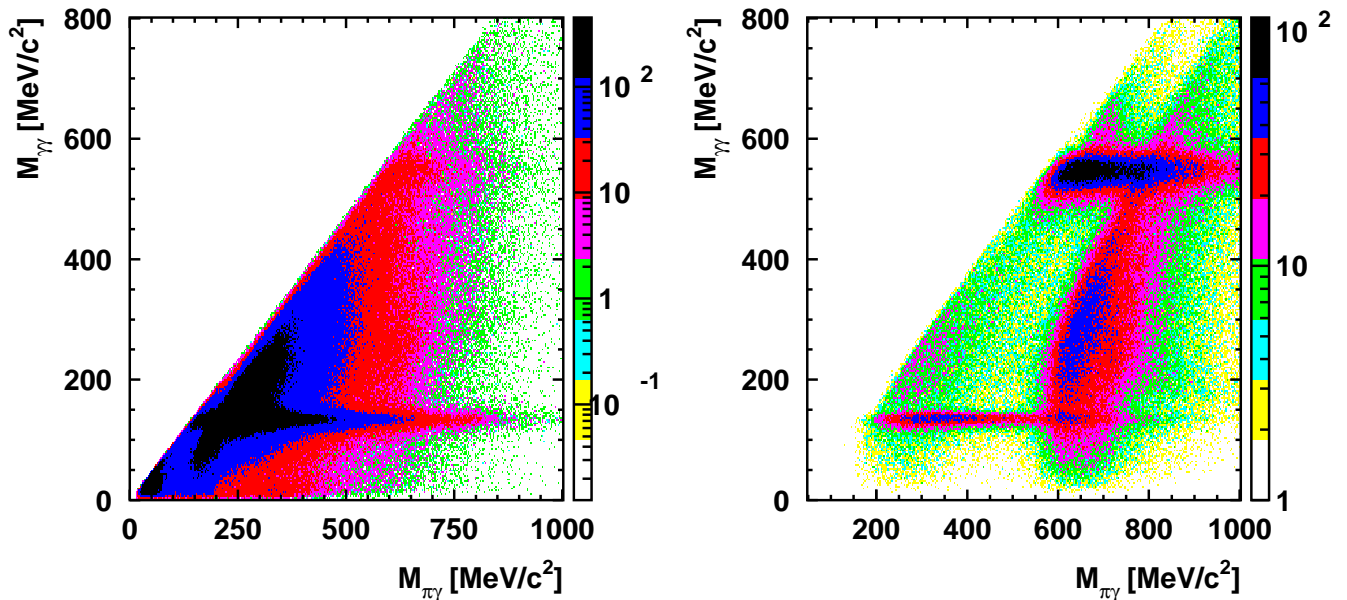


FIG. 5. (Color online) Left: Experimental data for the reaction $\gamma Nb \rightarrow Xp3\gamma$: the invariant mass of 2 photons (all 3 $\gamma\gamma$ combinations) versus the $\pi^0\gamma$ invariant mass. On the x-axis only one value is plotted per event for the 3 γ combination with the best π^0 . Right: Monte Carlo simulation: corresponding plot for the reaction $\gamma p \rightarrow p\pi^0\eta$. Only those events are plotted where 1 proton and 3 photons are registered.

inate time accidental background. Random time coincidences were subtracted using events outside the prompt time coincidence window. For this analysis the prompt peak was between -3 and 7 ns (Fig. 4a) and only events within the prompt peak were accepted as candidates for the reactions of interest. The asymmetric time cut allowed photons as well as nucleons to trigger the event. Photons registered in TAPS were required to be prompt within -2.5 to 2.5 ns (Fig 4b).

3. Split-off

Monte Carlo simulations have shown that there is a strong contribution to the 3 γ invariant mass spectrum from single η photoproduction $\eta \rightarrow \gamma\gamma$, which has a huge cross section at energies 900-1100 MeV. Shower fluctuations may result in an additional isolated energy deposit which is then reconstructed as an additional photon. Due to this split-off of one photon cluster, 3 PED's are registered. With a high probability this process occurs in the transition zone between the detectors TAPS and Crystal Barrel (Fig. 1 left). The photons from split-off events are in most cases of low energy. It is possible to suppress such events by applying the following cuts:

- 1) The detectors in the TAPS to CB transition zone at angles between 26° and 34° are excluded from the analysis, as well as the detectors for $\theta > 155^\circ$. According to simulations this leads to a 15% loss in the ω signal.
- 2) The energy threshold in each photon cluster is set to 50 MeV.

As a result of both cuts the background is reduced by

21%.

4. ω reconstruction

The ω meson was reconstructed and identified via the three photon final state invariant mass. Since the ω meson sequentially decays according to $\omega \rightarrow \pi^0\gamma \rightarrow \gamma\gamma\gamma$, the reconstructed particle can only be an ω meson if two of the three photons stem from a π^0 decay. According to the relation

$$E^2 = m^2 + p^2 \quad (2)$$

the π^0 and ω mesons have been identified via

$$m_{\pi^0} = \sqrt{2E_{\gamma 1}E_{\gamma 2}(1 - \cos\theta)}; \quad (3)$$

$$m_{\omega} = \sqrt{(E_{\pi^0} + E_{\gamma 3})^2 - (\vec{p}_{\pi^0} + \vec{p}_{\gamma 3})^2} \quad (4)$$

Thus in a two-dimensional plot of the two photon invariant mass (all 3 combinations) against the $\pi^0\gamma$ invariant mass, the ω meson should appear in this plane at the π^0 mass (2γ axis) and the ω mass ($\pi^0\gamma$ axis). Such a plot is shown in Fig. 5 left, where all cuts described so far have already been applied.

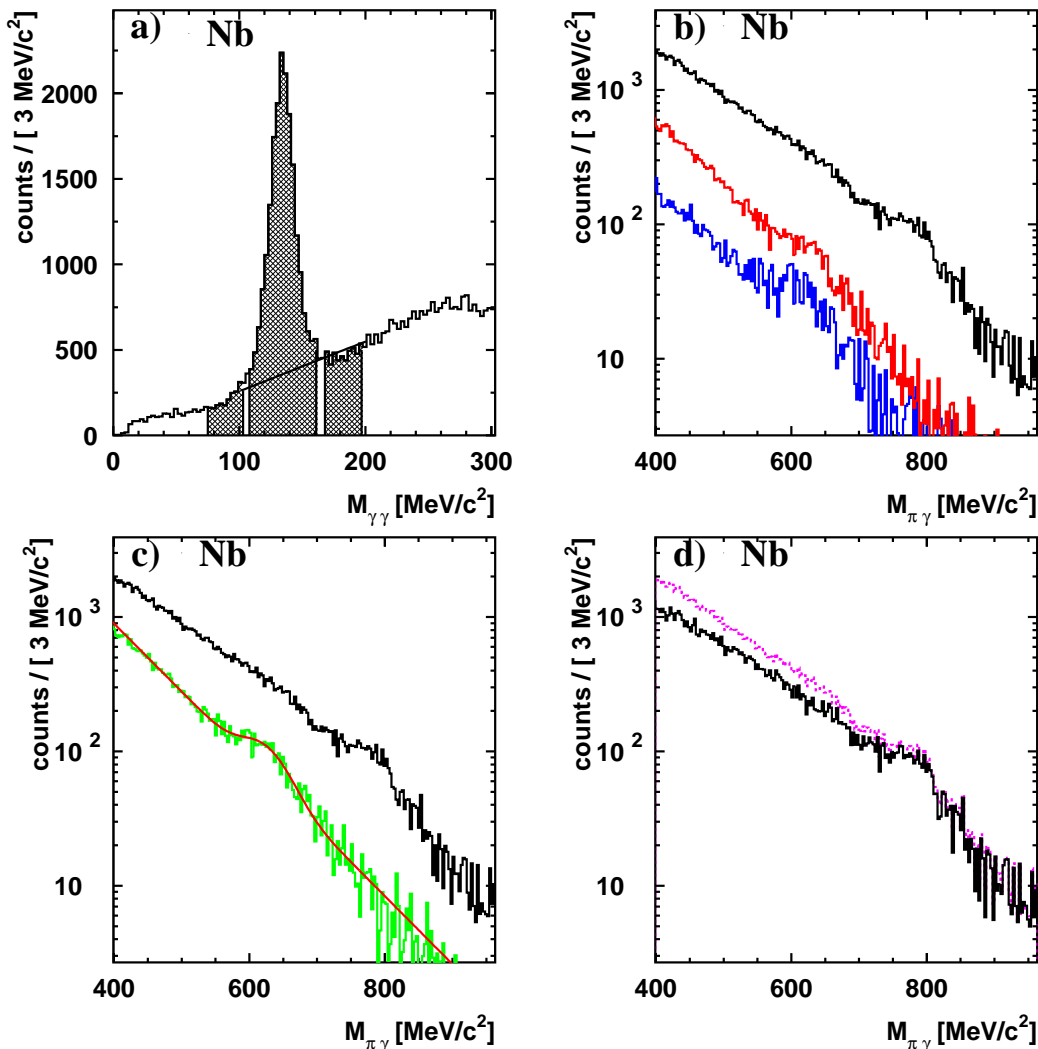


FIG. 6. (Color online) a) Invariant mass of two γ 's; y-projection of Fig. 5 left for a cut of $M(\pi^0\gamma)$ between 570 and 630 MeV. The shaded areas show the cuts for sideband subtraction. b) The $M(\pi^0\gamma)$ invariant mass distribution for the π^0 peak (black) and left (blue) and right (red) from the peak position as shown in a). c) The $\pi^0\gamma$ invariant mass in the π^0 peak (black) and the sum of the $M(\pi^0\gamma)$ projections left and right from the peak. The solid curve is a fit to the summed background spectrum. d) The $\pi^0\gamma$ invariant mass distribution after side band subtraction (solid histogram) compared to the spectrum without sideband subtraction (dashed histogram). All spectra refer to the Nb target.

5. Sideband subtraction technique

As mentioned above, one of the channels which contribute to the background is $\pi^0\eta$ photoproduction with 4 photons in the final state when one of the photons escapes detection. In order to suppress this background in the $\pi^0\gamma$ spectrum the technique of side band subtraction was used. Monte Carlo simulations (Fig. 5 right) show that events obtained by combining 2 γ 's from an η decay with a γ coming from a π^0 decay appear as an almost vertical band around 600 MeV on the x-axis, which shows up as a bump in the $M(\pi^0\gamma)$ projection.

To reduce this bump and to suppress the combinatorial background, side band subtraction has been applied. Fig. 6a shows the projection on the y-axis $M(\gamma\gamma)$ for the

mass range $570 \leq M(\gamma\gamma) \leq 630$ MeV. Projections on the x-axis $M(\pi^0\gamma)$ are shown in Fig. 6b for cuts close to the pion mass: 110 to 160 MeV and left (75 to 100 MeV) and right (170 to 195 MeV) from the peak. The sum of both sideband spectra (Fig. 6c) was normalized to the background counts under the pion peak and fitted with an exponential and Gaussian function. In the next step this curve was subtracted from the $M(\pi^0\gamma)$ spectrum over the full mass range. Fig. 6d shows the resulting spectrum after the sideband subtraction. The bump around 600 MeV is removed from the final spectrum. The background in the spectrum for masses of 400 MeV to 700 MeV is 37% lower compared to the spectrum without sideband subtraction, but the difference in the region of the ω signal from 700 MeV to 820 MeV is only

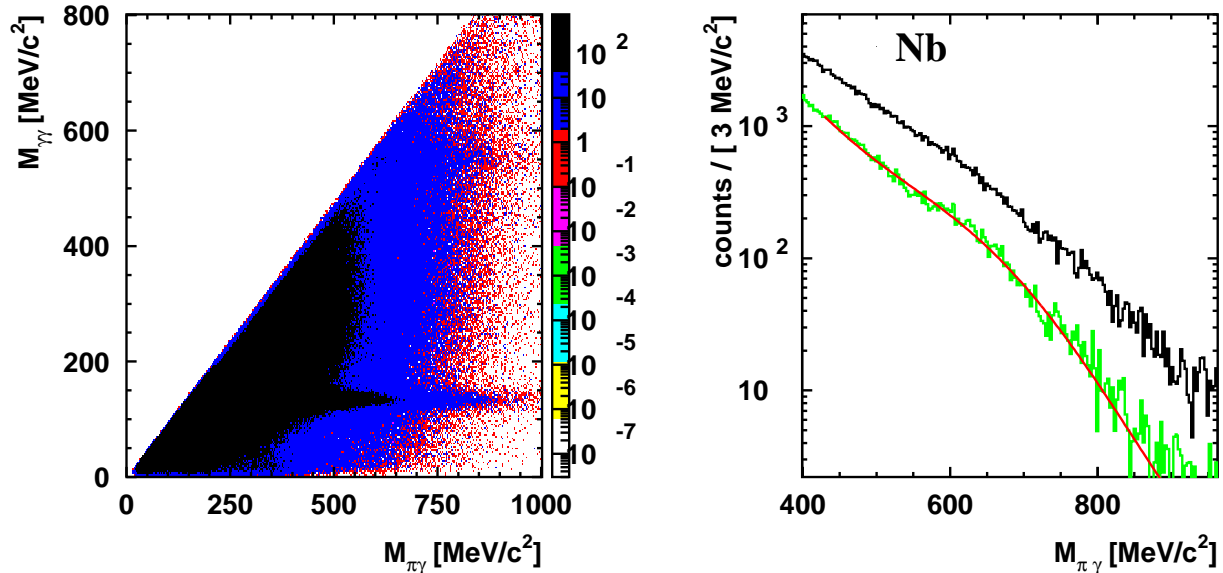


FIG. 7. (Color online) Left: Experimental data for the reaction $\gamma Nb \rightarrow Xp4\gamma$: after omitting one of the photons the invariant mass of 2 photons is plotted versus the $\pi^0\gamma$ invariant mass. On the x-axis only one value is plotted per event for the 3 γ combination with the best π^0 . Right: The $\pi^0\gamma$ invariant mass in the π^0 peak (black) and the sum of the $M(\pi^0\gamma)$ projections left and right from the peak. The solid curve is a fit to the summed background spectrum.

14% (Fig. 6d). It is essential to remove this structure arising from the $\pi^0\eta$ channel as it extends towards higher masses where it may distort the ω line shape.

6. Momentum cut

Only ω mesons decaying inside the nucleus carry information on the in-medium properties which are to be studied. To enhance the in-medium decay probability, the vector meson decay length should be comparable to nuclear dimensions. This was achieved in the analysis by applying a kinematic cut on the three momentum of the ω meson $|\vec{p}_\omega| \leq 500$ MeV/c. But still, only a fraction of the ω mesons will decay inside the nucleus. Thus, one expects the $\pi^0\gamma$ invariant mass spectrum to show a superposition of decays outside of the nucleus at the vacuum mass with a peak position at 782 MeV/c² and of possibly modified decays inside the nucleus [21]. In addition, the most pronounced in-medium effects are expected for low meson momenta with respect to the the nuclear medium.

7. Cut on the kinetic energy of the π^0 in the final state

The disadvantage of reconstructing the ω meson in the decay mode $\omega \rightarrow \pi^0\gamma$ is a possible rescattering of the π^0 meson which was studied in [21]. The authors have

demonstrated that the constraint on the pion kinetic energy $T_{\pi^0} > 150$ MeV suppresses the final state interaction down to the percent level in the invariant mass range of interest ($650 \text{ MeV} \leq M(\pi^0\gamma) \leq 850 \text{ MeV}$). This result has been confirmed in transport calculations [13], [22].

D. Background Analysis

The next main step in the analysis was the determination of the background directly from the data and its absolute normalization.

1. Background reconstruction

As mentioned before, the most probable sources of background come from the reactions $\gamma A \rightarrow (A-1)p\pi^0\pi^0$ and $\gamma A \rightarrow (A-1)p\pi^0\eta$ with 4 γ and one proton in the final state. Due to photon cluster overlap or detection inefficiencies one of the four photons may not be registered, thereby giving rise to a $\pi^0\gamma$ final state, which is exactly identical and therefore not distinguishable from the ω meson final state. To study this background, 5 PED events were selected with 4 neutral and 1 charged hit. One of the four neutral particles was randomly omitted and from the remaining photons a π^0 was identified and combined with the 3rd photon. The 2-dimensional plot of mass $M_{\gamma\gamma}$ versus the $\pi^0\gamma$ invariant mass is shown

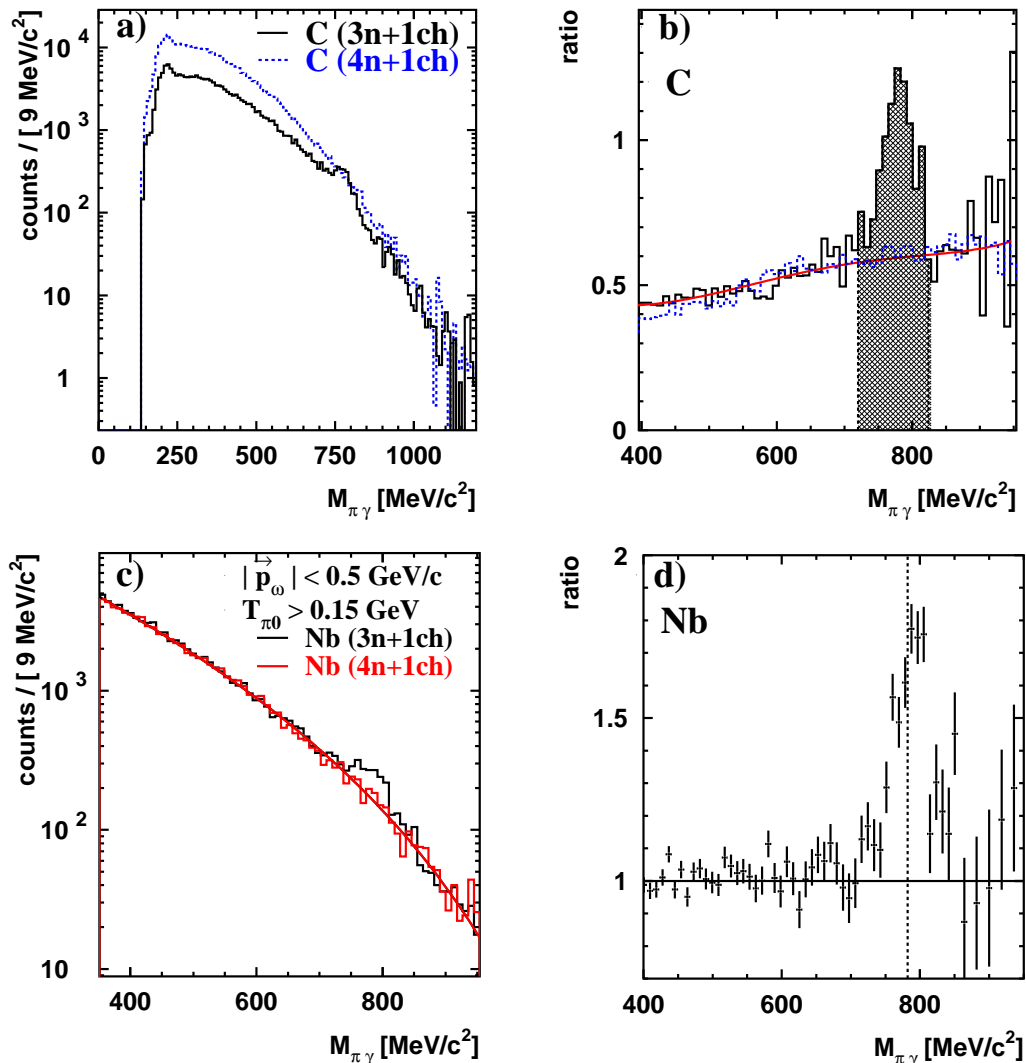


FIG. 8. (Color online) a) $\pi^0\gamma$ signal (solid curve) and background spectrum (dotted curve) for the C target deduced from events with 4 neutral and 1 charged hit. b) Correction function derived from the carbon data. The dashed curve shows the mass dependence of this correction expected from a simulation of the $2\pi^0$ channel. c) The $\pi^0\gamma$ signal spectrum and the corrected and normalized background spectrum for the Nb target. The solid curve represents a fit to the background distribution. d) Ratio of the $\pi^0\gamma$ spectrum to the background spectrum for the Nb target generated from events with 4 neutral and 1 charged hit.

in Fig. 7 (left). It is similar to the plot from the 4 PED events for the ω reconstruction (see Fig. 5 left). This is filled four times for all combinations with 4 photons. The side band subtraction technique was applied as described in sec. III C 5. The applied cuts on the $\pi^0\gamma$ momentum, on the kinetic energy of the pion and on the prompt peak were the same as for the ω meson reconstruction. The resulting $\pi^0\gamma$ spectrum is shown in Fig. 7 (right).

2. Lost photons

The slopes in the signal and background (BG) spectra shown in Fig. 8a are different due to the differ-

ent kinematics in detecting events with 4 neutral and 1 charged particle with respect to events with 3 neutral and 1 charged hits, reflecting the energy dependence of the probability that only 3 out of 4 photons are detected. The ratio of both spectra is shown in Fig. 8b for the C target. A procedure has been developed to correct the background slope in the Nb spectrum using the data obtained on the carbon target which is such a light nucleus that strong in-medium effects are not expected. The correction function is derived by fitting the ratio of the spectra for the carbon data excluding the peak region, as it is shown in Fig. 8b. The dependence of this correction on the $\pi^0\gamma$ invariant mass is confirmed by simulations (dashed curve in Fig. 8b) studying the en-

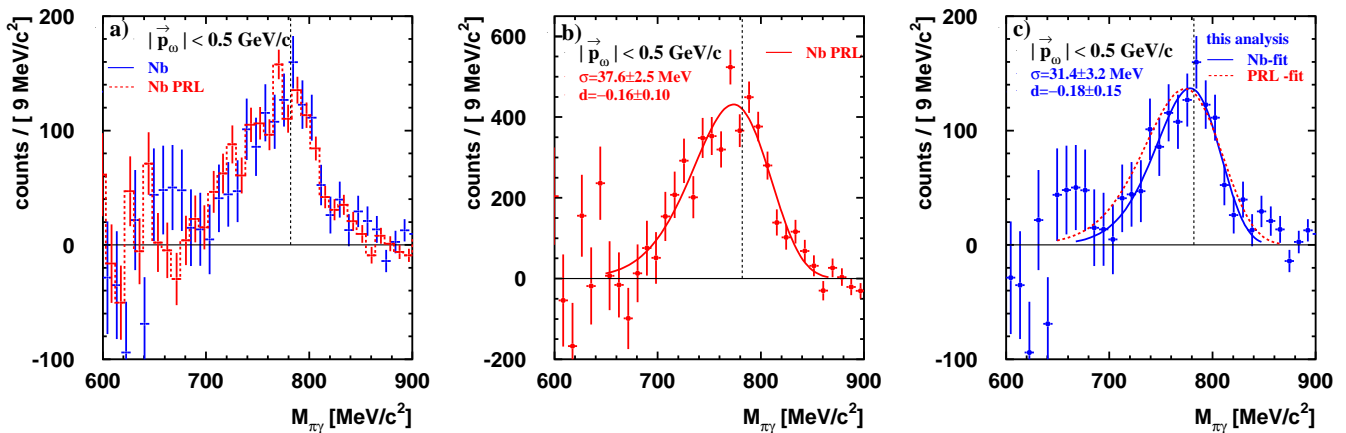


FIG. 9. (Color online) a) ω signal for the Nb target from this analysis (solid points) compared to the ω signal published in [1] (dashed). For the comparison of the line shapes the latter data have been scaled down by factor of 3.3 to match the intensity of the signal in the current analysis where more restrictive cuts have been applied. The spectra are without cut on the pion kinetic energy. b) fit to the ω signal published in [1] using the function given by Eq. 5. c) fit to the ω signal obtained in this analysis using the same function. The fit to the signal from [1] is included for comparison as red dashed line.

ergy dependence of the probability to register only 3 out of 4 photons for the dominating $2\pi^0$ background channel. The $\pi^0\gamma$ background for Nb from events with 4 neutral and 1 charged particles is multiplied with this correction function. As a result, the background for the Nb data changes its slope.

3. Background normalization

The absolute height of the background is determined by requesting the same number of counts for the signal and background spectra in the mass range from 400 to 960 MeV, excluding the counts in the ω peak which account for only 2% of the total yield in the given mass range. Thereby, the background level is fixed without paying any attention to the ω signal region. Fig. 8c shows the $\pi^0\gamma$ and the corrected and normalized background spectra. The ratio of these two spectra given in Fig. 8d demonstrates that the background in the $\pi^0\gamma$ spectrum on Nb is properly reproduced by the background spectrum generated from the events with 4 neutral and 1 charged hits after applying the required corrections. In the invariant mass range from 400 to 700 MeV the average deviation from unity is 4%. For higher invariant masses fluctuations become stronger because of the poorer statistics.

E. Results and Discussion

The ω signal shown in Fig. 9a is obtained by subtraction of the background from the signal spectrum. For comparison the ω line shape deduced in the previous analysis [1] is overlaid. Only slight differences are observed which, however, become more apparent when the

signals are fitted individually, as shown in Fig. 9b,c. The following function [23] has been used for the fits:

$$f(x) = A \cdot \exp \left[-\frac{1}{2} \left(\frac{\ln q_x}{d} \right)^2 + d^2 \right] \quad (5)$$

where

$$q_x = 1 + \frac{(x - E_p)}{\sigma} \cdot \frac{\sinh(d\sqrt{\ln 4})}{\sqrt{\ln 4}} \quad (6)$$

Here A is the amplitude of the signal, E_p is the peak energy, σ is FWHM/2.35 and d is the asymmetry parameter. This function takes into account the tail in the region of lower invariant masses resulting from the energy response of the calorimeters. Fig. 9 compares the fit to the ω signal published in [1] (Fig. 9b) with the fit to the ω signal obtained in this work (Fig. 9c). In the re-analysis a somewhat narrower ω signal is observed.

Applying in addition the cut on the kinetic energy of the π^0 meson ($T_{\pi^0} > 150$ MeV) a fit to the ω signal (Fig. 10a) yields a width parameter $\sigma = 25.7 \pm 2.4$ MeV which is consistent within errors with the LH_2 and MC signals (Fig. 10b,c) which serve as a reference. The deviation from the reference signals claimed in [1] and interpreted as evidence for an in-medium mass shift of the ω meson is thus not confirmed in the re-analysis of the data described in this paper. The current analysis does not yield any evidence for an in-medium lowering of the ω mass. This does not necessarily mean that there is no mass shift because the ω line shape may be insensitive to in-medium modifications as pointed out in [13].

This problem is illustrated in Fig. 11 which compares the ω line shape of the present analysis to the line shape for the LH_2 target as well as to a prediction of the ω line

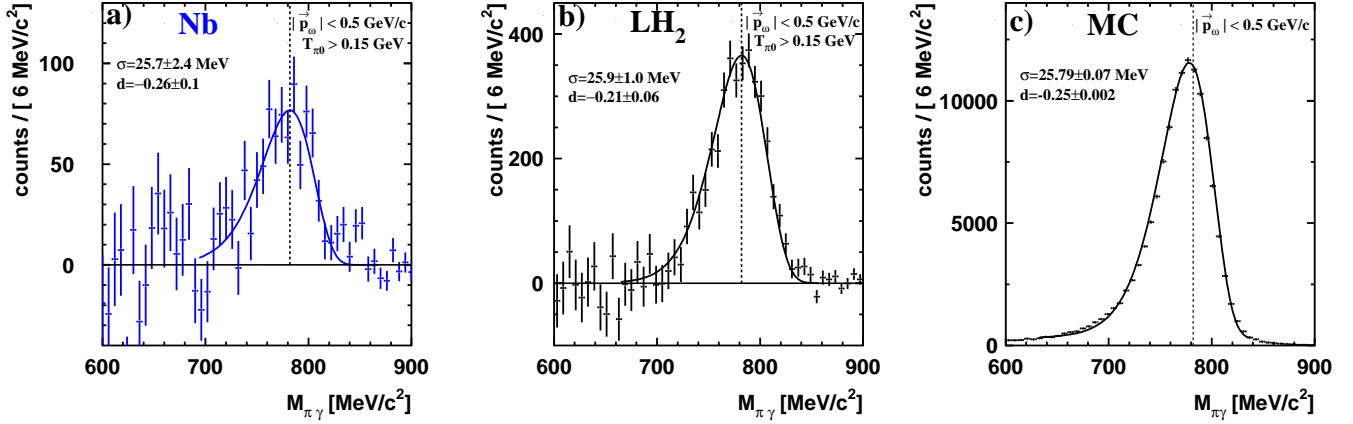


FIG. 10. (Color online) a) ω signal for $\pi^0\gamma$ momenta below 500 MeV/c and kinetic energy $T_{\pi^0} > 150$ MeV (*Nb* target). The solid curve represents a fit with the function of Eq. 5. b) ω signal for a *LH₂* target and c) ω signal from MC simulation.

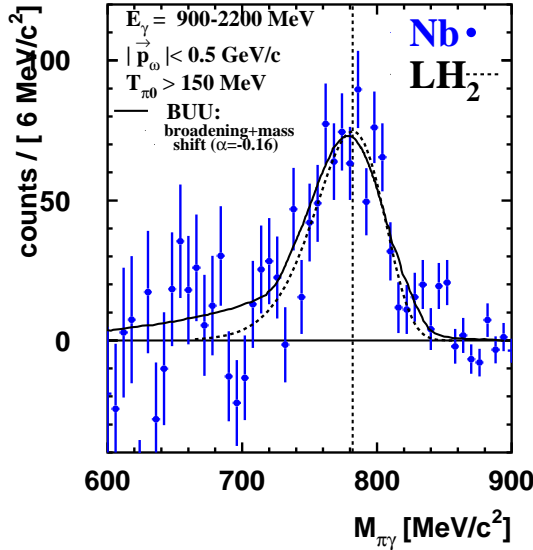


FIG. 11. (Color online) ω signal for the *Nb* target from this analysis (solid points) in comparison to the ω line shape measured on a *LH₂* target (dashed curve) and to a GiBUU simulation [24] (solid curve) assuming a mass shift by -16% at normal nuclear matter density.

shape in a GiBUU transport model calculation. In this calculation an in-medium pole mass shift according to

$$m_{\omega}^* = m_{\omega}^0 \left(1 - 0.16 \frac{\rho_N}{\rho_0}\right) \quad (7)$$

has been assumed. Here, ρ_N is the nuclear density at the decay point of the ω meson and ρ_0 is the normal nuclear matter density. The fact that the experimental signal is consistent with both scenarios indicates that the line

shape is indeed insensitive to in-medium modifications for the given invariant mass resolution and statistics.

This insensitivity is first of all due to the relatively long lifetime of the ω meson. Even requiring the ω recoil momentum to be lower than 500 MeV/c, only about 20% of all $\omega \rightarrow \pi^0\gamma$ decays in *Nb* occur at densities $\rho/\rho_0 > 0.1$ for the given reaction kinematics according to BUU simulations [24]. In addition, due to inelastic processes like $\omega N \rightarrow \pi N$, the ω mesons are removed in the nuclear medium thereby reducing their effective lifetime and correspondingly increasing their width. If this broadening is very large as observed for the ω meson [11] the strength of the in-medium signal is spread out in mass so strongly that it becomes hard to distinguish it from the background.

This argument can also be formulated more rigorously as discussed in [8, 25]. Any mass distribution measurement of a vector meson V from its decay into particles p_1, p_2 does not give the hadronic spectral function of the meson directly but folded with the branching ratio $\Gamma_{V \rightarrow p_1+p_2}/\Gamma_{\text{tot}}$ into the specific final channel one is investigating [26]

$$\frac{d\sigma_{\gamma N \rightarrow N(p_1, p_2)}}{d\mu} = \frac{d\sigma_{\gamma N \rightarrow V N}}{d\mu} \times \frac{\Gamma_{V \rightarrow p_1+p_2}(\mu)}{\Gamma_{\text{tot}}}. \quad (8)$$

Since the branching ratio may depend on the mass μ the unfolding is not trivial. Integrating Eq. 8 over all nucleons and parameterizing the spectral function $A(\mu)$ by a Breit-Wigner function, the result involves the term

$$A(\mu) \frac{\Gamma_{V \rightarrow \text{final state}}}{\Gamma_{\text{tot}}} = \frac{1}{\pi} \frac{\mu \Gamma_{\text{tot}}}{(\mu^2 - m_V^2)^2 + \mu^2 \Gamma_{\text{tot}}^2} \frac{\Gamma_{V \rightarrow \text{final state}}}{\Gamma_{\text{tot}}}. \quad (9)$$

Here Γ_{tot} is the total width of the meson V , obtained as a sum of the vacuum decay width, Γ_{vac} , and an in-medium contribution Γ_{med} :

$$\Gamma_{\text{tot}} = \Gamma_{\text{vac}} + \Gamma_{\text{med}} \quad (10)$$

with

$$\Gamma_{\text{med}}(\rho(r)) = \Gamma_{\text{med}}(\rho_0) \frac{\rho(r)}{\rho_0}. \quad (11)$$

in the low density approximation. Due to the second factor in Eq. 9 the meson decay into the channel of interest will decrease for a strong broadening of the meson in the nuclear medium. Furthermore, according to the first factor in Eq. 9 this reduced yield is spread out over a broader mass range, making it much more difficult to separate the in-medium decay contribution from the background. Moreover, since $\Gamma_{\text{tot}} \sim \rho/\rho_0$ for $\Gamma_{\text{med}} \gg \Gamma_{\text{vac}}$ the second factor in Eq. 9 becomes proportional to $\frac{1}{\rho/\rho_0}$, leading to a suppression of contributions from higher densities. The sensitivity of meson production in an elementary reaction is thereby shifted to the nuclear surface. In case of a strong in-medium broadening of a meson it is thus *in principle* difficult to detect in-medium modifications by an analysis of the signal shape. As a consequence the experiment becomes less sensitive to a possible mass shift. Requesting a proton in coincidence with 3 photons does not shift the sensitivity to even smaller densities. According to GiBUU simulations the fraction of $\omega \rightarrow \pi^0\gamma$ decays at densities larger than $0.1\rho_0$ is thereby changed only by less than 2% for the kinematic conditions of the current analysis [27].

It should be pointed out, however, that a significant effect close to the production threshold of the ω meson, $E_\gamma=1109$ MeV, was nevertheless predicted by the GiBUU model [28]. A data analysis confined to this energy regime is under way and will be published separately.

IV. SUMMARY AND CONCLUSIONS

Data on the photoproduction of ω mesons on LH_2 , C , and Nb have been re-analyzed, applying an improved

background determination and subtraction method. An earlier claim of an in-medium lowering of the ω mass is not confirmed. The strong broadening of the ω meson in the nuclear medium due to inelastic processes - as determined in a transparency ratio measurement - suppresses contributions to the observed ω signal from the interior of the nucleus. The branching ratio for in-medium decays into the channel of interest is drastically reduced. Thereby, the sensitivity is shifted to the nuclear surface, making the line shape analysis less sensitive to a direct observation of in-medium modifications. Data with much higher statistics will be needed to gain further insight. A corresponding experiment has been performed at the MAMI C electron accelerator using the Crystal Ball/TAPS detector setup. The analysis is ongoing.

ACKNOWLEDGMENTS

We thank the scientific and technical staff at ELSA and the collaborating institutions for their important contribution to the success of the experiment. We acknowledge detailed discussions with M. Kaskulov, U. Mosel, P. Mühlich, E. Oset and J. Weil. This work was supported financially by the *Deutsche Forschungs Gemeinschaft* through SFB/TR16. The Basel group acknowledges support from the *Schweizerischer Nationalfond* and the KVI group from the *Stichting voor Fundamenteel Onderzoek der Materie (FOM)* and the *Nederlandse Organisatie voor Wetenschappelijk Onderzoek (NWO)*.

-
- [1] D. Trnka *et al.*, Phys. Rev. Lett. **94**, 192303 (2005).
 - [2] D. J. Gross, Proc. Nat. Acad. Sci. **102**, 9099 (2005).
 - [3] H. D. Politzer, Proc. Nat. Acad. Sci. **102**, 7789 (2005).
 - [4] F. Wilczek, Proc. Nat. Acad. Sci. **102**, 8403 (2005).
 - [5] S. Dürr *et al.*, Science **322**, 1224 (2008).
 - [6] R. Rapp, J. Wambach, and H. van Hees, arXiv:0901.3289, Landolt-Börnstein New Series I-23/A(2009).
 - [7] R. Hayano and T. Hatsuda, arXiv:0812.1702(2009).
 - [8] S. Leupold, V. Metag, and U. Mosel, arXiv: 0907.2388, Int. J. Mod. Phys. **E 19**, 147 (2010).
 - [9] M. Naruki *et al.*, Phys. Rev. Lett. **96**, 092301 (2006).
 - [10] R. Arnaldi *et al.*, Eur. Phys. J. C. **49**, 235 (2007).
 - [11] M. Kotulla *et al.*, Phys. Rev. Lett. **100**, 192302 (2008).
 - [12] T. Ishikawa *et al.*, Phys. Lett. B **608**, 215 (2005).
 - [13] M. Kaskulov, E. Hernandez, and E. Oset, Eur. Phys. J. A **31**, 245 (2007).
 - [14] E. Aker *et al.*, Nucl. Instr. and Methods A **321**, 69 (1992).
 - [15] R. Novotny *et al.*, IEEE Trans. Nucl. Sci. **38**, 392 (1991).
 - [16] A. R. Gabler *et al.*, Nucl. Instr. and Meth. A **346**, 168 (1994).
 - [17] D. Husmann and W. J. Schuille, Phys. Bl. **44**, 40 (1988).
 - [18] W. Hillert, Eur. Phys. J. A **28**, 139 (2006).
 - [19] D. Elsner *et al.*, Eur. Phys. J. A **33**, 147 (2007).
 - [20] G. Suft *et al.*, Nucl. Instr. Meth., A **538**, 416 (2005).
 - [21] J. G. Messchendorp *et al.*, Eur. Phys. J. A **11**, 95 (2001).
 - [22] P. Mühlich, T. Falter, and U. Mosel, Eur. Phys. J. A **20**, 499 (2004).
 - [23] B. Aubert *et al.*, Phys. Rev. D **70**, 112006 (2004).
 - [24] P. Mühlich, PhD thesis, Univ. of Giessen(2006).
 - [25] J. Lehr and U. Mosel, Phys. Rev. C. **64**, 042202 (2001).
 - [26] F. Eichstädt *et al.*, Prog. Theo. Phys. Suppl. **168**, 495 (2007).
 - [27] S. Friedrich, University of Giessen, priv.com., <http://gibuu.physik.uni-giessen.de>(2010).

- [28] K. Gallmeister, M. Kaskulov, U. Mosel, and P. Mühlich, Prog. Part. Nucl. Phys. **61**, 283 (2008).